LIQUID CRYSTALS, 1995, VOL. 19, NO. 4, 459–467

Isotropic–cholesteric phase transition in colloidal suspensions of filamentous bacteriophage *fd*

by JIANXIN TANG and SETH FRADEN*
Martin Fisher School of Physics, Brandeis University, Waltham, Massachusetts 02254, U.S.A.

(*Received 28 March 1994; accepted 15 April 1994*)

The co-existence concentrations of the isotropic and cholesteric liquid crystalline phases of the semi-flexible rod-like virus *fd* in aqueous suspension were measured as a function of ionic strength at room temperature. At several ionic strengths the magnetic-field-induced birefringence, which is proportional to the number of particles in a correlation volume N_{corr}, was measured for *fd* concentrations spanning the entire isotropic region. From this data the limiting concentration of stability (spinodal) of the isotropic phase, ρ^*, was obtained. The co-existence concentrations and ρ^* versus ionic strength compare well with predictions based on the theory of Khokhlov and Semenov, modified to include the effects of charge. A theoretical expression for the magnetic birefringence of persistent polymers was derived and agreed well with the data with the exception that N_{corr} at the isotropic to liquid crystal transition was smaller than predicted.

1. Introduction

In this paper, we report extensive measurements on the isotropic–cholesteric phase transition in the model colloidal system, filamentous bacteriophage *fd*, a semi-flexible rod-like virus. This virus has a large length to diameter ratio of 140, and an isotropic–cholesteric transition is observed at volume fractions of 0·5–2 per cent. A statistical mechanical theory of an isotropic to nematic phase transition of hard particles was first developed by Onsager [1]. He noted that at very low concentrations a colloidal suspension of rods approximates an ideal gas and that an expansion of the free energy in the powers of concentration provides a theory of the phase transition whose accuracy increases with the ratio of the length to diameter of the particles. The unique attribute of using a virus particle as an experimental system for investigating the Onsager theory is that nature has designed the rod-like virus particles to be identical in structure, which gives rise to same physical parameters such as mass, length, diameter, as well as charge density in solution. Such a high degree of monodispersity is not currently obtainable using synthetic chemical methods.

While the theory of the co-existence of isotropic and nematic phases described by Onsager applies to colloidal suspensions of rigid and charged rod-like particles, similar liquid crystalline transitions also occur with long semi-flexible polymers [2]. In an attempt to provide a unified theoretical model, Khokhlov and Semenov (KS) [3] generalized Onsager's approach to include systems of semi-flexible chains of contour length (L) much greater than the particle diameter (D), and for arbitrary persistence length (P). Khokhlov and Semenov solved their model explicitly only in the limit of $L \gg P$, and many of the theories and experiments in this area have been reviewed by Vroege and Lekkerkerker [4] in 1992. More recently, Chen [5] has reported an accurate numerical calculation of the KS model for concentrations of the co-existing isotropic (ρ_i) and anisotropic (ρ_a) phases, as well as the order parameter (S) of the ordered phase at the isotropic–anisotropic (I–A) phase transition for hard particles of arbitrary flexibility. In this paper, the orientationally anisotropic phase (A) refers to either the nematic, or cholesteric phase. In a cholesteric, the nematic alignment direction rotates in a helical fashion and the pitch of a cholesteric is defined as the distance along the screw axis in which the local director has rotated by 360 degrees. Since a typical *fd* cholesteric has a pitch much larger than the intermolecular spacing, the energy of twist in the cholesteric contributes only a minute perturbation to the total energy associated with the parallel alignment of the molecules [6, 7]. One therefore expects that any theory of the isotropic–nematic phase transition will be equally applicable to the isotropic–cholesteric transition.

Experimentally, the properties of the nematic or cholesteric phases have been extensively investigated in a variety of rod-like colloidal suspensions, such as monodisperse Tobacco Mosaic Virus (TMV) [8–11],

* Author for correspondence.

filamentous bacteriophage *fd* and its close relative *M13* [12–14], poly(γ-benzyl glutamate) (PBG) [15–18], poly(hexyl isocyanate) (PHIC) [19–21], schizophyllan [22–24], xanthan [25,26], as well as DNA molecules [27–29]. Among the measured properties are the isotropic–nematic (cholesteric) co-existence concentrations as a function of aspect ratio L/D [16,21,22], persistence length (P) [20,21], ionic strength (I) [11,25,26], and temperature [15,20,27], the angular distribution function of the anisotropic phase [10], the osmotic pressure as a function of concentration [16,18,21,24], and the second virial coefficient or excluded volume [8,9,14,28,29]. A series of measurements of co-existence concentrations have been performed by Teramoto, Sato and co-workers [20–26]. They have studied a variety of polymer systems, both neutral and charged, and of different values of L/D, P/L, and ionic strength I. In general, good agreement between theory and experiment is found, although with some notable exceptions, such as a measured co-existence region much wider than predicted by theory for aqueous solutions of xanthan [25]. The best agreement with theory among the systems they studied seems to be obtained with solutions of PHIC in toluene with $P \approx L$ [20].

In our study, we employed the *fd* virus, which is of length 880 nm (L) and diameter 6·6 nm (D) [30,32], with an approximate charge density of 10 e nm^{-1} at pH 7·5 [33] and molecular weight $1{\cdot}64 \times 10^7$ g mol^{-1} [30]. We tried to characterize sample polydispersity using electron microscopy (EM) and analytical centrifugation. However, each of these techniques have their limitations. *fd* is thin and flexible and the extreme conditions of EM tend to both fragment and aggregate particles leading to an apparent increase in polydispersity. On the other hand, the extreme length of particles leads to hydrodynamic interactions between *fd* particles in suspension, which cause the distributions as determined by analytical centrifugation to appear more monodisperse than actually. One indirect assay of the length distribution is that we observed a smectic phase in samples of 3–10 per cent volume fraction as a function of ionic strength. Since slight polydispersity suppresses the smectic phase, we conclude that the viruses are highly monodisperse.

The persistence length (P) of *fd* is 2200 nm, which is about 2·5 times its contour length and has been determined by light scattering and electron microscopy studies [34–37]. Previous studies have shown that the *fd* suspensions form a cholesteric liquid crystalline phase at about 1 to 2 per cent in volume fraction [12–14] depending on the ionic strength. The well-characterized physical properties of *fd* make it an ideal particle for testing co-existence theories for the case of intermediate rigidity, especially the recent numerical solution to the Khokhlov–Semenov theory [5].

2. Phase co-existence

2.1. *Theory*

Our discussion starts with the virial expansion of the free energy per particle of a dilute suspension of hard, semi-flexible polymers [4]

$$\frac{F(f)}{kT} = \text{const.} + \ln c' + \sigma(f) + c'\rho(f), \qquad (1)$$

where f is the orientational distribution function, $c' = (\pi/4)L^2Dn$ is the dimensionless concentration with n the number density of particles, $\sigma(f)$ is the orientational entropy, which has known analytical expressions only at the extremely rigid ($P \gg L$) and the long worm-like ($L \gg P$) limits [3], and $\rho(f) = (4/\pi)\int\int |\sin\gamma| f(\Omega) f(\Omega')\, d\Omega\, d\Omega'$ is the excluded volume term where γ is the angle between long axes of two interacting rods. The osmotic pressure and the chemical potential can both be derived from equation (1) and are used to obtain the co-existence concentrations between an isotropic and an orientationally ordered phase.

While the co-existence concentrations of hard rod-like particles of arbitrary flexibility have been obtained numerically, the case of charged rods is yet to be solved. Onsager demonstrated that the dominant effect of charge is to modify the excluded volume term in the free energy expansion and introduced a charge-dependent effective diameter D_{eff}, larger than the hard rod diameter D. D_{eff} is calculated by finding the separation of the rods at which the energy of repulsion equals kT as averaged over the angular distribution function (f) in the isotropic phase [1]. Stroobants *et al.* [38], have shown that there is a smaller additional factor in determining the co-existence concentrations, which scales as $h = \kappa^{-1}/D_{\text{eff}}$, the ratio of the Debye screening length to the effective diameter. This constant is known as the 'twist' parameter. The modified free energy expansion is, after introducing the effective diameter and adding a 'twist' term $\eta(f)$ to the excluded volume [38]

$$\frac{F(f)}{kT} = \text{const.} + \ln c + \sigma(f) + c[\rho(f) + h\eta(f)], \qquad (2)$$

where

$$c = \frac{\pi}{4} L^2 D_{\text{eff}}$$

and

$$\eta(f) = -\frac{4}{\pi}\int\int |\sin\gamma| \ln|\sin\gamma|\, d\Omega d\Omega' - (\ln 2 - \tfrac{1}{2})\rho(f). \qquad (3)$$

Physically, $\eta(f)$ accommodates the fact that two rods with fixed separation between their centres of mass have a lower energy when their axes are perpendicular rather than parallel.

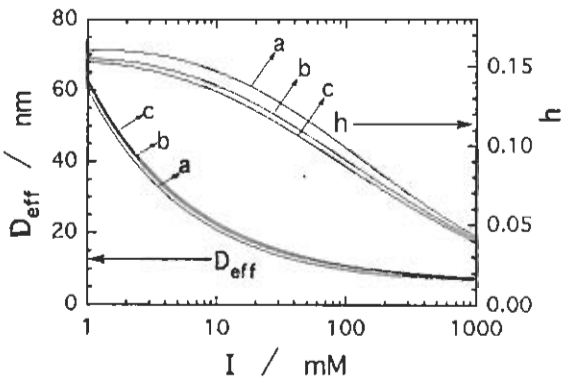

Figure 1. Effective diameter (D_{eff}) and twist parameter (h) as functions of ionic strength (I). Both D_{eff} and h decrease monotonically with increasing I; D_{eff} approaches the bare diameter of 6·6 nm for the *fd* virus at high ionic strength. Three charge densities were chosen: (*a*) $5\,e\,nm^{-1}$, (*b*) $10\,e\,nm^{-1}$, and (*c*) $20\,e\,nm^{-1}$. At these high charge densities D_{eff} and h are insensitive to the variation in charge.

In figure 1, we plot D_{eff} and h calculated as described by Stroobants *et al.* [38] as functions of ionic strength with assumed charge densities of $5\,e\,nm^{-1}$, $10\,e\,nm^{-1}$, and $20\,e\,nm^{-1}$ for *fd* particles. Solution of the Poisson–Boltzmann equation was obtained by a numerical calculation, following the procedure as described by Philip and Wooding [39]. Since h is small, we can apply the numerical results of Chen for the co-existence concentrations, which are calculated for neutral rods ($h = 0$), to our charged system by scaling the co-existence concentrations with D_{eff} rather than D. The conversion between the dimensionless co-existence concentrations $c_{i,a}$ and mass densities $\rho_{i,a}$ is, $\rho_{i,a} = m(4c_{i,a}/\pi L^2 D_{eff})$, with m the mass of a *fd* particle. Here, $c_{i,a}$ are calculated using equation (3.10) and equation (3.11) in the paper of Chen [5], with the coefficients given in table III therein, and $\alpha = L/2P = 0{\cdot}2$ for *fd*.

2.2. *Measurements*

A *fd* virus solution of 6 per cent volume fraction was dialyzed against Tris–HCl buffer solutions at room temperature (23 ± 1°C) and pH 7·5 of ionic strengths from 0·85 mM to 850 mM. Since the pK of Tris at 25°C is 8·3, we calculated that at pH 7·5 approximately 85 per cent of the Tris molecules in solution were protonated into monovalent positive ions and charge neutralized by the Cl^- ions. The samples of the virus suspensions were then carefully diluted to the co-existence region and allowed sufficient time to phase-separate in small clean glass tubes of roughly 40 mm × 5 mm size. At high ionic strength, which leads to high co-existence concentrations, the samples were rather viscous and the phase separation in the bulk becomes so slow that a table centrifuge was used to apply up to 1000 g to speed the separation after the isotropic and anisotropic (I–A) phases segregated to the scale of microns by standing at 1 g overnight. All measurements in this report were performed at room temperature.

Samples of volume 20 μl or so were carefully taken by pipette from both the isotropic phase at the top and the cholesteric phase at the bottom, with the phases clearly identified by examination through crossed polarizers. The samples were then immediately weighed with an analytical balance of 0·01 mg accuracy. Subsequently, each was diluted 20 to 100 fold to measure the *fd* concentration by optical spectrophotometry with absorption coefficient $3{\cdot}84\,ml\,mg^{-1}$ at 269 nm [40]. Repeated measurements indicated a precision of about 2 per cent for the same sample. However, the variation between different samples prepared with the same conditions occasionally reached 5 per cent. This small scatter of the I–A co-existence concentration data may be attributed to slight polydispersity in the *fd* stock, but also partially to the fact that the co-existence concentrations slowly shift higher with time. The shift appears faster at lower ionic strength. In 1 mM Tris–Cl, for example, it reaches a couple of per cent in about a week and the trend slows down several weeks after the sample is brought into room temperature. The physical origin of this phenomenon is not understood. At 4°C the sample remains quite stable for months.

Since the concentration difference between isotropic and anisotropic phases is only about 10 per cent, we selected to measure ρ_i and ρ_a in the same samples and used only the samples prepared within a week or two from stable refrigerated stock to eliminate the two primary causes of error as mentioned above. It should also be mentioned here that since the flexibility of *fd* particles is sensitive to temperature, co-existence concentrations also change with temperature, unlike tobacco mosaic virus (TMV), which is athermal [11]. The temperature dependence of the flexibility and the co-existence concentrations of *fd* will be the subject of a separate paper.

Figure 2 (*a*) shows ρ_i and ρ_a each as a function of ionic strength. Theoretical curves are from the numerical results of Chen [5] as described in the last section with D_{eff} taken from figure 1. Experimental data shown in the figure and listed in table 1 were only up to 170 mM ionic strength above which serious aggregation was observed through the increase in scattering of the suspension. Although no free parameters are used in the comparison of theory and experiment, we note that D_{eff} is calculated assuming $10\,e\,nm^{-1}$. However, D_{eff} is insensitive to the value of the charge density for the range of values consistent with titration measurements [33]. The theory also ignores the twisting term $\eta(f)$ (equation (3)), and we expect the inclusion of this effect would shift the theoretical co-existence region to slightly greater concentrations.

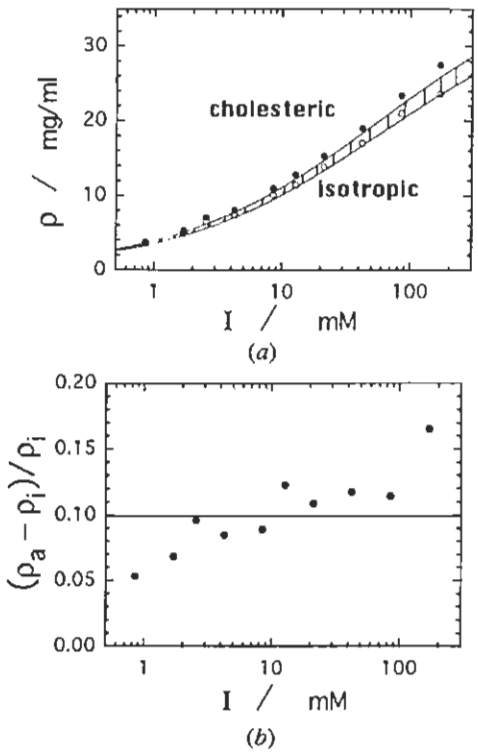

Figure 2. (*a*) Phase boundary concentrations of *fd* suspension in co-existence of the isotropic and the cholesteric phase versus ionic strength (I). Theory curves are calculated based on numerical results from Chen [5] by taking $L/P = 0{\cdot}4$ and the effective diameter from figure 1 with charge density assumed to be $10\,e\,nm^{-1}$. Vertical bars indicate the co-existence region. (*b*) Plots of the ratio $\omega = (\rho_a - \rho_i)/\rho_i$ at different ionic strengths. The numerical result, ignoring the twisting effect ($h = 0$), predicts $\omega = 0{\cdot}099$ (solid line). See table 1 for a list of experimental data.

Table 1. Co-existence concentrations ($\rho_{i,a}$) as function of ionic strength.

I/mM	ρ_i/mg ml^{-1}	ρ_a/mg ml^{-1}	ω/per cent
0·85	3·6	3·8	5·3
1·7	5·0	5·3	6·8
2·55	6·5	7·1	9·6
4·3	7·4	8·0	8·5
8·5	10·1	11·0	8·9
12·8	11·4	12·8	12·3
21·3	13·8	15·3	10·9
42·5	17·0	19·0	11·8
85	21·0	23·4	11·4
170	23·6	27·5	16·5

In figure 2 (*b*), the measured difference of the co-existence concentrations relative to ρ_i, $\omega = (\rho_a - \rho_i)/\rho_i$, is plotted as a function of ionic strength I. Despite the experimental error we have repeatedly measured the ratio ω to average approximately 10 per cent. This is at least twice as large as the value from the Khokhlov and Semenov interpolation [3] but falls into close agreement with Chen's numerical result, which is $\omega = 9{\cdot}9$ per cent for $L/2P = 0{\cdot}2$. The co-existence width ω increases as ionic strength varies from 0·85 to 170 mM. This suggests the need to include the twisting effect (equation (3)) in the calculation of the co-existence concentrations. The smallest values of ω occur at the lowest ionic strengths where the twisting constant h is the largest. This is reasonable since large values of h act to destabilize the nematic phase [38, 40].

3. Magnetic birefringence study

3.1. *Theory*

If a molecule has an anisotropy of the diamagnetic susceptibility $\Delta\chi$, then in the presence of a magnetic field H, there is an additional term in the free energy expansion of equation (2), $\Delta F = -1/3\Delta\chi H^2 S$ [6], where $S = \int f(\theta) P_2(\theta)\, d\Omega$ [42] is the orientational order parameter with $P_2(\theta)$ the second order Legendre polynomial, θ being the angle between the particle long axis and the direction of the field. If the particle is semi-flexible, one can write the field energy term identically as above, with $\Delta\chi$ the anisotropy of the fully straightened polymer molecule, and S the order parameter averaged along the entire persistent chain.

In the limit of weak alignment, or equivalently in the limit that $\Delta\chi H^2/kT \to 0$, one can expand the free energy expression keeping only up to the quadratic term of the order parameter S [3, 9, 11, 38]. By minimizing the free energy, we obtain the following expression for the field-induced order parameter [42] for charged persistent polymers derived in the appendix

$$S = \frac{\Delta\chi H^2}{15kT} \frac{\dfrac{2}{3N}\left[1 - \dfrac{1}{3N}(1 - \exp(-3N))\right]}{1 - \dfrac{c}{6N}\left[1 - \dfrac{1}{3N}(1 - \exp(-3N))\right](1 - 3h/4)} \tag{4}$$

where $N = L/P$ is the ratio of contour to persistence length, $c = (\pi/4)L^2 D_{eff} n$ is the dimensionless polymer concentration, and h is the twist parameter introduced earlier. This expression for the order parameter contains the full dependence of charge, in contrast to the co-existence concentrations where the twisting constant h was set to zero.

Experimentally, one can measure the optical birefringence and in the limit that $H^2 \to 0$ obtain the Cotton–Mouton (CM) constant [41], $K_{CM} = \Delta n/\lambda H^2$. Since $\Delta n = \Delta n_{sat} S$ with Δn_{sat} the birefringence of a completely aligned suspension, an expression similar to equation (4)

holds for the specific Cotton–Mouton constant K_{CM}/ρ, with ρ the mass concentration

$$\frac{\rho}{K_{CM}} = \frac{\rho}{K_{CM}}\bigg|_{\rho\to 0}\left\{1 - \frac{\rho}{\tilde{\rho}}\frac{2}{3N}\left[1 - \frac{1}{3N} \times (1 - \exp(-3N))\right](1 - 3h/4)\right\}, \quad (5)$$

where

$$\tilde{\rho} = m\frac{16}{\pi D_{\text{eff}} L^2}$$

and

$$\frac{\rho}{K_{CM}}\bigg|_{\rho\to 0} = \frac{15kT\lambda}{C\Delta\alpha\Delta\chi}\left\{\frac{2}{3N}\left[1 - \frac{1}{3N}(1 - \exp(-3N))\right]\right\}^{-1} \quad (6)$$

with $\Delta\alpha$ and $\Delta\chi$ the anisotropies of optical polarizability and magnetic susceptibility for a fully straightened polymer, and C a proportionality constant introduced in the appendix. Equation (6) has been derived earlier from a different treatment [43].

In an isotropic suspension of finite concentration, although the orientation of molecules is globally isotropic, locally molecules have angular correlation with neighbours. The ratio between the specific Cotton–Mouton constant at a finite concentration, $\mathbf{K}_{CM}/\rho$, and at the dilute limit. $\mathbf{K}_{CM}/\rho|_{\rho\to 0}$, is a measure of the degree of angular correlation [11]

$$N_{\text{corr}} = \frac{\mathbf{K}_{CM}/\rho}{\mathbf{K}_{CM}/\rho}\bigg|_{\rho\to 0}. \quad (7)$$

N_{corr} can be interpreted as the number of particles in a correlation volume, and from here on we shall simply call N_{corr} the angular correlation number.

One can introduce ρ^* as the concentration at which the isotropic phase becomes absolutely unstable. ρ^*, which is also known as the isotropic branch of the spinodal, is obtained from equation (5) and equals

$$\rho^* = \tilde{\rho}\Big/\left\{\frac{2}{3N}\left[1 - \frac{1}{3N}(1 - \exp(-3N))\right](1 - 3h/4)\right\} \quad (8)$$

and thus from equations (5)–(8)

$$N_{\text{corr}} = (1 - \rho/\rho^*)^{-1}. \quad (9)$$

We see that N_{corr} diverges as the concentration is increased towards ρ^*.

3.2. *Experimental*

Magnetic field induced optical birefringence measurements were performed at the Francis Bitter National Magnet Laboratory. We used a photoelastic modulation and 2-lock-in amplification set-up [44]. The measured field induced phase shift $\Delta\varphi$ [41] is related to the orientational order parameter S and the field induced birefringence Δn as follows:

$$S = \frac{\Delta n}{\Delta n_{\text{sat}}} = \frac{\lambda\Delta\varphi}{2\pi d\Delta n_{\text{sat}}}, \quad (10)$$

where $\lambda = 633$ nm, $d = 3{\cdot}0$ mm is the sample pathlength, and Δn_{sat} is the birefringence of the *fd* sample in full alignment.

3.3. *Results*

We have measured the field induced birefringence (Δn) of *fd* solutions over the entire concentration range of the isotropic phase. We find that Δn is proportional to the square of the magnetic field H^2 for dilute samples with field up to 20 Tesla. For all concentrations, the specific Cotton–Mouton constant $\mathbf{K}_{CM}/\rho$ was determined from the initial linear response of Δn as a function of H^2, as shown in figure 3. However, for the most concentrated samples at high field, a large non-linear increase in Δn with H^2 was observed and eventually saturation of Δn occurred. This

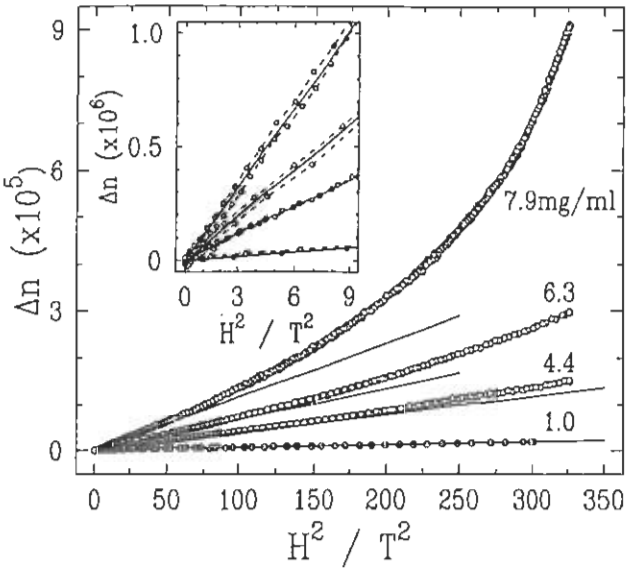

Figure 3 The magnetic field induced birefringence Δn, as a function of field squared H^2[Tesla^2], at four representative concentrations. The open circles (○) are the experimental data, and the solid lines are linear fits of data at low fields (0–3 T), except for the lowest concentration (1·0 mg ml^{-1}), for which the linear fit was applied to the entire field range. The upper left window is a magnified display of the same data at low field. The open circles (○) are connected by dotted lines with the data below the solid lines taken as the field increased and the data above taken as the field decreased. The birefringence is linear in H^2 at all concentrations in the limit of weak field. The large non-linear increase in Δn for the highest concentration is indicative of a field-induced phase transition [45]. All the samples were at Tris-Cl buffer at pH 7·5, with the ionic strength approximately 5 mM.

and further evidence of a field-induced isotropic–nematic phase transition are discussed elsewhere [45]. The buffer used among the group of samples reported in figure 3 was Tris–Cl at about 5 mM ionic strength and pH 7·5. The same behaviour of the concentration dependence has been observed with several other ionic strengths as well.

We measured the Cotton–Mouton constant of isotropic *fd* solutions of five ionic strengths. Our measurements extend the previous work by Nakamura and Okano who made the first study of pretransitional angular correlations in colloidal nematics using *fd* at a single ionic strength [14]. Figure 4 (*a*) shows the inverse of the specific CM constant versus ρ. These data were fit to equation (9) for each ionic strength to obtain the concentration ρ^* where the orientational interparticle correlation diverges. Isotropic solutions of concentration ρ^* are not obtained experimentally, since a first order I–A transition spontaneously occurs at $\rho_i < \rho^*$. At each ionic strength, $K_{CM}/\rho|_{\rho\to 0}$ is determined by extrapolating the data from figure 4 (*a*) to zero concentration. The average value of $K_{CM}/\rho|_{\rho\to 0}$ is $(0{\cdot}9 \pm 0{\cdot}1) \times 10^{-4}\,T^{-2}\,cm^2\,mg^{-1}$, which agrees very well with the value of $(0{\cdot}97 \pm 0{\cdot}05) \times 10^{-4}\,T^{-2}\,cm^2\,mg^{-1}$ reported previously by Torbet and Maret [41]. However, in the work of Nakamura and Okano, the Cotton–Mouton constants for dilute solutions were found to be about two-thirds of the values mentioned above [14].

Among the data measured at the five ionic strengths, the specific Cotton–Mouton constant at the dilute limit, $\mathbf{K}_{CM}/\rho|_{\rho\to 0}$, is shown to vary by 10 per cent. The variation was found to have no systematic dependence on the ionic strength from repeated measurements of different samples prepared at different ionic strengths, or, in some cases, in different buffer solutions of potassium or sodium phosphate at pH 7·3 instead of Tris-Cl. We also performed measurements of the specific Cotton–Mouton constant in the dilute limit ($\mathbf{K}_{CM}/\rho|_{\rho\to 0}$) with samples made from a single concentrated stock solution of *fd* as a function of ionic strength. The samples were made by diluting the stock 100 fold into the final ionic strength solutions, and $\mathbf{K}_{CM}/\rho|_{\rho\to 0}$ was determined immediately upon dilution. No dependence on the ionic strength I was observed. We therefore conclude that the variation in $\rho/K_{CM}|_{\rho\to 0}$ seen in figure 4 (*a*) arises from other causes related to sample history. In a previous report [11], a similar occurrence was observed with TMV solutions where the variation in $\rho/K_{CM}|_{\rho\to 0}$ had no systematic dependence on I.

Note also in figure 4 (*a*), the low ionic strength data (0·85 mM, 1·7 mM) show slight curvature, reminiscent of that shown in TMV solutions reported by Fraden *et al.* [11], due to the contribution of higher virial terms. This is consistent with the TMV data, since with the increase of D_{eff} as the ionic strength decreases, the effective aspect ratio of *fd* drops to about 15, comparable to that of TMV. However, such a drop of the aspect ratio should also affect the co-existence concentrations, which is not incorporated in the theory curves of figure 2 (*a*).

In figure 4 (*b*), the ratio between the specific Cotton–Mouton constant at finite concentration K_{CM}/ρ, and in the dilute limit $K_{CM}/\rho|_{\rho\to 0}$, is plotted as a function of *fd*

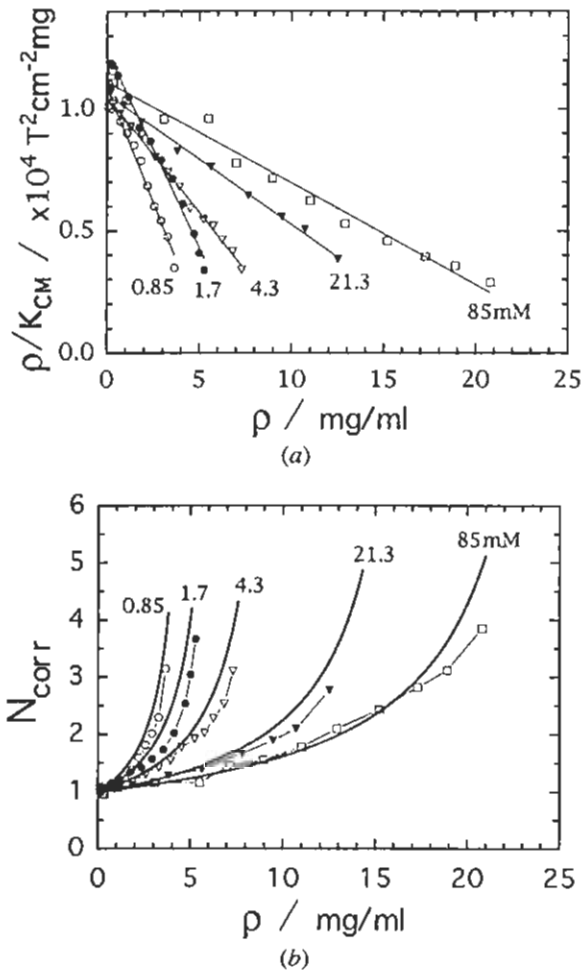

Figure 4. (*a*) The inverse of the specific Cotton–Mouton constant $\rho/\mathbf{K}_{CM}$ versus *fd* concentration ρ. The five curves correspond to the five ionic strengths labeled on the plot in units of milli-molar (mM) with the buffer being Tris-Cl at pH 7·5. In all cases the highest concentration is at the isotropic–cholesteric(I–A) phase transition. Each group of data is fit to equations (9) and extrapolated to obtain ρ^*, which is the concentration where $\rho/K_{CM} = 0$. The average value of the five specific Cotton–Mouton constants is $K_{CM}/\rho|_{\rho\to 0} = (0{\cdot}9 \pm 0{\cdot}1) \times 10^{-4}\,T^{-2}\,cm^2\,mg^{-1}$. (*b*) The concentration dependence of the ratio of the specific Cotton–Mouton constant $\mathbf{K}_{CM}/\rho$, measured at finite concentrations, and $\mathbf{K}_{CM}/\rho|_{\rho\to 0}$, obtained from (*a*). This ratio is equal to the correlation number N_{corr} (equation (7)). Experimentally, N_{corr} varies between 2·5 and 4 at the I–A transition. In contrast to (*a*), the solid lines are drawn using the theoretical ρ^* and ρ_i values with no adjustable or fit parameters.

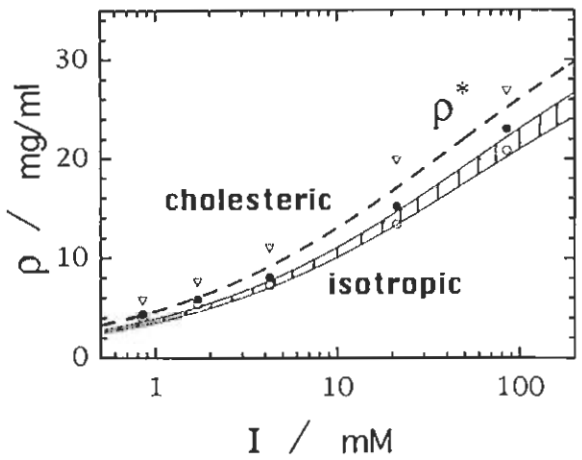

Figure 5. The experimental co-existence concentrations of the isotropic and cholesteric phases ρ_i(○), ρ_a(●), and the limit of stability (spinodal) of the isotropic phase ρ^*(▽), plotted at five ionic strengths. The calculated ρ_i and ρ_a (solid curves) are the same as in figure 2 (*a*), while the calculated ρ^* (dashed line) is from equation (8). Experimental data are also listed in table 2.

concentration at each ionic strength. This ratio is equal to the angular correlation number N_{corr} as we discussed in § 3.1. $K_{CM}/\rho|_{\rho\to 0}$ is obtained from figure 4 (*a*) through a linear fit of the experimental data. We also plotted theoretical curves of N_{corr} as a function of concentration, with values of ρ^* calculated from equation (8) and ρ_i calculated from [5] ignoring the twisting term $\eta(f)$ (equation (3)) in the free energy. At ρ_i, the theoretical value of N_{corr} is about five with some variation depending on ionic strength. This variation results from the inclusion of the twist parameter h, which factors into the expression of ρ^* in equation (8). Experimentally, however, N_{corr} ranges between 2·5 and 4·0 for the highest possible concentration, which occurs when there is a co-existence of the isotropic and cholesteric phases. In our comparison of the theory and the experimental measurement of N_{corr}, we divide K_{CM}/ρ by $K_{CM}/\rho|_{\rho\to 0}$, obtained through experimental measurement so that N_{corr} is 1 at the zero concentration limit. Despite the similarity in curvature, almost all the experimental data reside below the corresponding theory curves. This is illustrated by a further comparison in figure 5, which shows that ρ^* obtained through experimental extrapolation in figure 4 (*a*) is systematically higher than the theoretical prediction of ρ^* from equation (8).

In figure 5, ρ^* obtained from the birefringence measurements is plotted with the corresponding co-existence concentrations ρ_i and ρ_a measured directly from the same stock used for the magnetic birefringence measurements. The theoretical curves for ρ_i and ρ_a are the same as in figure 2 (*a*) and ρ^* is calculated from equation (8). Experimental data are listed in table 2. Note that the co-existence concentrations are different than those in table 1. These differences are mainly due to the fact that some measurements (0·85 mM, 1·7 mM, and 21·3 mM) were performed earlier in the project, when the ionic strength of solutions was not as precisely controlled as later when the measurements in table 1 were performed. The co-existence concentrations are very sensitive to variation in ionic strength at low salt.

Table 2. Co-existence concentrations ($\rho_{i,a}$) in comparison with limiting concentration of stability (ρ^*), as function of ionic strength (I).

I/mM	ρ_i/mg ml^{-1}	ρ_a/mg ml^{-1}	ρ^*/mg ml^{-1}	ρ_i/ρ^*
0·85	4·0	4·4	5·7	0·70
1·7	5·4	5·9	7·6	0·70
4·3	7·4	8·1	11·0	0·66
21·3	13·4	15·2	19·8	0·68
85	20·8	23·0	26·8	0·78

It is clearly shown that ρ^* (the spinodal) lies outside the phase co-existence region at all ionic strengths as predicted by theory. However, the comparison of ρ^* with theory seems less satisfactory than that of the co-existence concentrations. Experimentally, the ratio ρ_i/ρ^* is about 0·7 for the five ionic strengths, while it would be about 0·8 from the existing predictions.

4. Conclusions

We have applied the recent numerical calculations [5] for the model of the isotropic–nematic phase transition of persistent polymers [3] to *fd* virus solutions and found good agreement between the predicted and measured co-existence concentrations for a variety of ionic strengths. A systematic variation in the width of the co-existence concentrations indicates the need to fully incorporate the effect of charge into the theory. The comparison between theory and experiment involved no adjustable parameters. A theoretical expression for the magnetic birefringence of charged persistent polymers was derived using the Khokhlov–Semennov free energy and agrees with the previously derived expression in the dilute limit. The spinodal of the isotropic phase ρ^*, obtained through magnetic birefringence studies, was 10 per cent greater than what is predicted, even when fully incorporating the charge effect. We have also determined that there is no change of flexibility as the ionic strength ranged from 0·85 mM to 170 mM by measuring the specific Cotton–Mouton constant as a function of ionic strength at low concentrations. These measurements further establish *fd* as a model system to investigate the phase behaviour, and the micro- and macroscopic order of suspension of charged semi-flexible rod-like molecules [48].

We thank E. Bullit, L. Makowski, M. Cahoon and Z. Dogic for assistance in the preparation of virus. We are indebted to D. L. D. Caspar for extensive usage of the facilities in the Rosenstiel Center for Biomedical Research. We thank Th. Odijk and Takahiro Sato for bringing errors in a preliminary version of this work to our attention, and Jining Han for helping correct the appendix. We acknowledge support from NSF-DMR 4-59850, and the Francis Bitter National Magnet Laboratory.

Appendix

The free energy expansion for a solution of charged semi-flexible macromolecules given in equation (2) has an additional term in the presence of a magnetic field

$$\frac{F(f)}{kT} = \text{const.} + \ln c + \sigma(f) + c[\rho(f) + h\eta(f)] - \frac{\Delta\chi H^2}{3kT} S, \tag{A 1}$$

where S is the orientational order parameter, and $\Delta\chi$ is the anisotropy of the magnetic susceptibility of a fully straightened polymer molecule. Other notations follow from equation (2) in § 2.1.

In the limit of weak alignment, the orientational distribution function $f(\Omega)$ can be expressed as [42]

$$f(\Omega) = \frac{1}{4\pi}[1 + 5SP_2(\theta)], \tag{A 2}$$

where $P_2(\theta)$ is the second order Legendre polynomial. We can expand $\sigma(f)$, $\rho(f)$, and $\eta(f)$ to the quadratic term of S [3, 9, 11, 38],

$$\sigma(f) = (5S^2/4)\frac{3N}{1-(1-\exp(-3N))/3N}, \tag{A 3}$$

$$\rho(f) = 1 - 5S^2/8, \tag{A 4}$$

and

$$\eta(f) = 15S^2/32, \tag{A 5}$$

with $N = L/P$, the ratio of the persistence length.

By minimizing the free energy, one obtains the field-induced order parameter for charged persistent polymers

$$S = \frac{\Delta\chi H^2}{15kT} \frac{\frac{2}{3N}\left[1 - \frac{1}{3N}(1-\exp(-3N))\right]}{1 - \frac{c}{6N}\left[1 - \frac{1}{3N}(1-\exp(-3N))\right](1-3h/4)}. \tag{A 6}$$

For the case of a rigid charged rod, given by $N \to 0$, one arrives at the previously determined expression [11]

$$S = \frac{\Delta\chi H^2}{15kT} \frac{1}{1 - \frac{c}{4}(1-3h/4)}. \tag{A 7}$$

In the long worm-like limit, $N \to \infty$, equation (A 6) leads again to equation (A 7) with the substitutions $\Delta\chi \to \Delta\chi_p$ and $c \to c_p$, where $\Delta\chi_p = (2/3N)\Delta\chi$ and $c_p = (2/3N)c$ are the magnetic anisotropy of a persistence segment and the dimensionless concentrations of persistent segments, respectively.

The order parameter S can be determined by the measurement of the field-induced birefringence, $\Delta n = \Delta n_{sat} S$, with Δn_{sat} the birefringence of a completely aligned polymer suspension. To relate Δn_{sat} of the suspension to the optical properties of individual macromolecules, it is natural to apply the Lorentz–Lorenz formula to the persistent polymer chains in full alignment [41]

$$\Delta n_{sat}/\rho = C\Delta\alpha \tag{A 8}$$

where $\Delta\alpha$ is the anisotropy of optical polarizability of a single polymer, and C is a simple proportionality constant.

For the case of the magnetic-field-induced birefringence, one measures the Cotton–Mouton constant K_{CM}

$$K_{CM} = (\Delta n\lambda H^2)|_{H\to 0}. \tag{A 9}$$

Combining equations (A 6), (A 8), and (A 9) leads to equation (5) in § 3.1. Equation (6) agrees with the previous result obtained through a different derivation [43, 46, 47].

References

[1] Onsager, L., 1949, *Ann. N.Y. Acad. Sci.*, **51,** 627.
[2] Flory, P. J. 1956, *Proc. R. Soc.* A, 234, **60,** 73.
[3] Khokhlov, A. R., and Semenov, A. N., 1982, *Physica.* A, **112,** 605.
[4] Vroege, G. J., and Lekkerkerker, H. W., 1992, *Rep. Prog. Phys*, **55,** 1241.
[5] Chen, Z. Y., 1993, *Macromolecules*, **26,** 3419.
[6] de Gennes, P. G., 1974, *The Physics of Liquid Crystals* (Clarendon, Oxford), Chap. 3.
[7] Chandrasekhar, S., 1977, *Liquid Crystals* (Cambridge University Press), Chap. 1.
[8] Oster, G., 1950, *J. gen. Physiol.*, **33,** 445.
[9] Photinos, P., Rosenblatt, C., Schuster, T. M., and Saupe, A., 1987, *J. chem. Phys.*, **87,** 6740.
[10] Oldenbourg, R., Wen, X., Meyer, R. B., and Caspar, D. L. D., 1988, *Phys. Rev. Lett.*, **61,** 1851.
[11] Fraden, S., Maret, G., Caspar, D. L. D., and Meyer, R. B., 1989, *Phys. Rev. Lett.*, **63,** 2068. Fraden, S., Maret, G., and Caspar, D. L. D., 1993, *Phys. Rev.* E, **48,** 2816.
[12] Lapointe, J., and Marvin, D. A., 1973, *Molec. Crystals liq. Crystals*, **19,** 269.
[13] Oldenbourg, R., 1981, Ph.D. Thesis, University of Konstanz, Germany.
[14] Nakamura, H., and Okano, K., 1983, *Phys. Rev. Lett.*, **50,** 186.
[15] Wee, E. L., and Miller, W. G., 1971, *J. phys. Chem.*, **75,** 1446. Russo, P. S., and Miller, W. G., 1982, *Macromolecules*, **16,** 1690.

[16] KUBO, K., and OGINO, K., 1979, *Molec. Crystals liq. Crystals*, **53,** 207. KUBO, K., 1981, *Molec. Crystals liq. Crystals*, **74,** 71.
[17] GORDON, M., 1984, *Advances in Polymer Science*, Vol. 59 (Springer-Verlag), p. 37.
[18] HENTSCHKE, R., 1990, *Macromolecules*, **23,** 1192.
[19] CONIO, G., BIANCHI, E., CIFERRI, A., and KRIGBAUM, W. R., 1984, *Macromolecules*, **17,** 856.
[20] ITOU, T., and TERAMOTO, A., 1988, *Macromolecules*, **21,** 2225.
[21] ITOU, T., SATO, T., and TERAMOTO, A., 1988, *Polymer. J.*, **20,** 1049.
[22] ITOU, T., and TERAMOTO, A., 1984, *Macromolecules*, **17,** 1419.
[23] ITOU, T., and TERAMOTO, A., 1984, *Polymer J.*, **16,** 779.
[24] SATO, T., and TERAMOTO, A., 1990, *Molec. Crystals liq. Crystals*, **178,** 143.
[25] SATO, T., KAKIHARA, T., and TERAMOTO, A., 1990, *Polymer*, **31,** 824.
[26] INATOMI, S., JINBO, Y., SATO, T., and TERAMOTO, A., 1992, *Macromolecules*, **25,** 5013.
[27] STRZELECKA, T. E., and RILL, R. L., 1987, *J. Am. chem. Soc.*, **109,** 4513. STRZELECKA, T. E., and RILL, R. L., 1990, *Biopolymers*, **30,** 57. STRZELECKA, T. E., and RILL, R. L., 1991, *Macromolecules*, **24,** 5124.
[28] NICOLAI, T., and MANDEL, M., 1989, *Macromolecules*, **22,** 438.
[29] BRIAN, A. A., FRISCH, H. L., and LERMAN, L. S., 1981, *Biopolymers*, **20,** 1305. TROHALAKI, S., BRIAN, A. A., FRISCH, H. L., and LERMAN, L. S., 1984, *Biophys. J.*, **45,** 777.
[30] NEWMAN, J., SWINNEY, H. L., and DAY, L. A., 1977, *J. molec. Biol.*, **116,** 593.
[31] DAY, L. A., MARZEC, C. J., REISBERG, S. A., and CASADEVALL, A., 1988, *Ann. Rev. Biophys. Biophys. Chem.*, **17,** 509.
[32] BHATTACHARJEE, S., GLUCKSMAN, M. J., and MAKOWSKI, L., 1992, *Biophys. J.*, **61,** 725.
[33] ZIMMERMANN, K., HAGEDORN, J., HEUCK, C. C., HINRICHSEN, M., and LUDWIG, J., 1986, *J. biol. Chem.*, **261,** 1653.
[34] SONG, L., KIM, U.-S., WILCOXON, J., and SCHURR, J. M., 1991, *Biopolymers*, **31,** 547.
[35] MAEDA, T., and FUJIME, S., 1985, *Macromolecules*, **18,** 2430.
[36] LOH, E., RALSTON, E., and SCHUMAKER, V. N., 1979, *Biopolymers*, **18,** 2549, and 2569.
[37] BECK, K., and DUENKI, R. M., 1990, *J. struct. Biol.*, **105,** 22.
[38] STROOBANTS, A., LEKKERKERKER, H. N. W., and ODIJK, TH., 1986, *Macromolecules*, **19,** 2232.
[39] PHILIP, J. R., and WOODING, R. A., 1970, *J. chem. Phys.*, **52,** 953.
[40] ODIJK, TH., 1986, *Macromolecules*, **19,** 2313.
[41] TORBET, J., and MARET, G., 1981, *Biopolymers*, **20,** 2657.
[42] STRALEY, J. P., 1973, *Molec. Crystals liq. Crystals*, **22,** 333.
[43] MARET, G., and WEILL, G., 1983, *Biopolymers*, **22,** 2727.
[44] LARSON, B., 1986, Ph.D. thesis, MIT, USA
[45] TANG, J., and FRADEN, S., 1993, *Phys. Rev. Lett.*, **71,** 3509.
[46] ARPIN, M., STRAZIELLE, C., WEILL, G., and BENOIT, H., 1977, *Polymer*, **18,** 262.
[47] NAGAI, K., and ISHIKAWA, T., 1965, *J. chem. Phys.*, **43,** 4508.
[48] FRADEN, S., *Observation and Prediction of Phase Transitions in Complex Fluids*, NATO-ASI Vol. CXXIX, edited by M. Baus, L. F. Rull and J. P. Ryckaert.